COBEM 2021 26th International Congress of Mechanical Engineering
ABCM Associação Brasileira de Engenharia e Ciências Mecânicas
November 22-26, 2021, Virtual Congress, Brazil

COB-2021-0998
PARAMETRIC POD-BASED MODEL ORDER REDUCTION OF MULTIBODY SYSTEM DYNAMICS BASED ON THE ABSOLUTE NODAL COORDINATE FORMULATION

Matheus Basílio Rodrigues Fernandes
Thiago de Paula Sales
Domingos Alves Rade
André Fernando de Castro da Silva
Aeronautics Institute of Technology, Pç. Mal. Eduardo Gomes, 50, São José dos Campos, SP 12228-900, Brazil
engmatheusb@gmail.com, tpsales@ita.br, rade@ita.br, andref@ita.br

Abstract. *The absolute nodal coordinate formulation (ANCF) is the state-of-art in the computational modeling of flexible multibody dynamics. However, as the accuracy requirements of the ANCF model become more stringent, or the number of bodies raises, the number of ANCF elements increases, bringing the model to be artificially high-dimensional. To improve the computational efficiency of the ANCF for large systems, a model order reduction based on the proper orthogonal decomposition (POD) and Galerkin projection is proposed. Also, to permit the reduced-order model (ROM) to be adaptative to the variation of system parameters, a methodology based on an interpolation of the ROMs in a manifold is used. Finally, two numerical examples of flexible systems undergoing large reference motions and large deformations are used to verify the accuracy of the proposed methodology.*

Keywords: *flexible multibody system dynamics, Absolute Nodal Coordinate Formulation, parametric model order reduction, proper orthogonal decomposition*

1. INTRODUCTION

Multibody dynamics is the subject concerned with the modeling and analysis of bodies that can undergo large displacements and rotations. It has been applied in numerous industrial and technological fields such as robotics, space structures, biomechanics, precision machines, mechanisms, and vehicle dynamics. Since many of these systems are traditionally built using stiff components, they have often been analyzed and designed within the framework of rigid body dynamics. However, with the development of lighter materials and the need for weight alleviation and higher operating speeds, it became necessary to develop methodologies that take into account the effect of the, possibly large, deformation of the system components on their own dynamics. This led to the field of flexible multibody dynamics, which has attracted increasing attention over the past three decades (Shabana, 1997b).

In the late nineties, Shabana and co-workers (Shabana, 1997a; Shabana *et al.*, 1998; Escalona *et al.*, 1998) proposed the Absolute Nodal Coordinate Formulation (ANCF) as an accurate and non-incremental finite element methodology to model flexible multibody systems subjected to both gross reference motion and large deformations. Since then, the ANCF has been recognized as a benchmark in the dynamical modeling of flexible multibody systems (Shabana, 2013).

A remarkable fact about the governing equations obtained using the ANCF is their high nonlinearity and large dimensionality. The nonlinearity arises due to the presence of finite rotations in the gross motion and the occurrence of large deformations. The high dimensionality, in turn, caused by the finite element discretization process in the space. Usually, as accuracy requirements become more strict, the resulting dimension of the model also increases.

In addition, some problems, such as the control of flexible robot arm systems, may require real-time simulations. An optimization analysis for flexible multibody dynamic systems, in turn, may require several repetitions of nonlinear structural analysis for each time step (Kim and Cho, 2018). To meet all of these requirements, a methodology that can increase the computational efficiency of the analysis of large-scale systems is mandatory.

One such methodology is the technique of reduced-order modeling. The fundamental idea of model order reduction is to replace the high dimensional full-order model (FOM) with a reduced-order model (ROM) that accurately captures the dynamics of the original system (Brunton and Kutz, 2019). One of such methods is the proper orthogonal decomposition (POD), which is a data-driven method capable of generating modes that are tailored specifically to the particular system. Based on the singular value decomposition (SVD), the POD generates a set of orthogonal modes (the POD modes) which is optimal, in the sense of the Eckart-Young theorem (Brunton and Kutz, 2019), for representing numerical and experimental data (Kerschen *et al.*, 2005).

However, the POD-based ROM can be constructed only after simulating the high-fidelity FOM. Hence, its usefulness is more evident when one needs to perform successive simulations, such as the case of dynamical simulations of a system with parameter variation. In this case, it is advantageous to build a parametric ROM, such that the modes obtained through the simulation of the FOM can be interpolated to capture the parameter variations (Amsallem and Farhat, 2008; Amsallem *et al.*, 2009).

In this context, this work presents a parametric POD-based model order reduction for the dynamics of multibody systems modeled in the framework of the absolute nodal coordinate formulation. First, in Sect. 2, the ANCF formulation is outlined for the beam element used in this study. It is also discussed the numerical method adopted to integrate the resulting set of differential and algebraic equations. In Sect. 3, the use of POD and Galerkin projection to reduce the dimensionality of the model is presented. Then, in Sect. 4, an adaptation of ROMs to new sets of parameters based on interpolation on a manifold is presented. In Sect. 5, the presented methodology is applied to two flexible systems, namely, a four-bar mechanism, and a free-falling double pendulum. Finally, some concluding remarks are outlined in Sect. 6.

2. BRIEF DESCRIPTION OF THE ANCF

In the ANCF formulation, no infinitesimal or finite rotations are used as nodal coordinates. Instead, absolute displacements and displacement gradients at the nodal points are used as the element nodal coordinates (Gerstmayr *et al.*, 2013). The kinematics of the ANCF element is expressed in terms of the shape function matrix $\mathbf{S}(\mathbf{x})$ and the vector of nodal coordinates, $\mathbf{e}(t)$. Using both, the global position vector of an arbitrary point on the ANCF element can be described as:

$$\mathbf{r}(t, \mathbf{x}) = \mathbf{S}(\mathbf{x})\mathbf{e}(t), \tag{1}$$

where $\mathbf{x}$ describes the position of the point in the local frame of coordinates of the element.

The mass matrix $\mathbf{M}^e$ of an ANCF element (which is always constant) can be derived as (Gerstmayr *et al.*, 2013):

$$\mathbf{M}^e = \int_V \rho\, \mathbf{S}^{\mathrm{T}}\mathbf{S}\, dV, \tag{2}$$

where ρ and V are the density and volume of the element, respectively.

The dynamic governing equations of a flexible multibody system can be expressed as a set of coupled differential and algebraic equations:

$$\begin{cases} \mathbf{M}\ddot{\mathbf{q}} + \mathbf{C}_{\mathbf{q}}^{\mathrm{T}}\boldsymbol{\lambda} = \mathbf{F}^{\mathrm{ext}}(t, \mathbf{q}, \dot{\mathbf{q}}) - \mathbf{F}^{\mathrm{int}}(\mathbf{q}) = \mathbf{Q}(t, \mathbf{q}, \dot{\mathbf{q}}) \\ \mathbf{C}(t, \mathbf{q}) = \mathbf{0} \end{cases} \tag{3}$$

where $\mathbf{M}$ is the mass matrix of the system, $\mathbf{F}^{\mathrm{int}}(\mathbf{q})$ is the highly nonlinear vector of internal forces, $\mathbf{C}_{\mathbf{q}} = \partial\mathbf{C}(t, \mathbf{q})/\partial\mathbf{q}$ is the Jacobian matrix of the kinematic constraints vector $\mathbf{C}(t, \mathbf{q})$, $\boldsymbol{\lambda}$ is the vector of Lagrange multipliers and $\mathbf{F}^{\mathrm{ext}}(t, \mathbf{q}, \dot{\mathbf{q}})$ is the vector of generalized external forces. The system's matrices and vectors are assembled from the individual matrices and vectors of the rigid and flexible bodies that make up the system through the use of a standard finite element procedure.

To solve the set of differential and algebraic equations of Eq. (3), the HHT-I3 implicit method is used. This method uses the traditional and well-known HHT (Hilber-Hughes-Taylor) method to transform the differential equations of motion into nonlinear algebraic equations (Negrut *et al.*, 2007, 2009). These are solved simultaneously with the nonlinear constraint equations using, for instance, an iterative Newton-Raphson method to determine the state of the system. The HHT-I3 integrator has adjustable numerical damping properties, while it remains stable and second order convergent (Arnold and Brüls, 2007).

Using the HHT method, the differential-algebraic equation system presented above can be recast as:

$$\begin{cases} \mathbf{F}^{(1)} = \dfrac{1}{1+\alpha}(\mathbf{M}\ddot{\mathbf{q}})_{n+1} + (\mathbf{C}_{\mathbf{q}}^{\mathrm{T}}\boldsymbol{\lambda} - \mathbf{Q})_{n+1} - \dfrac{\alpha}{1+\alpha}(\mathbf{C}_{\mathbf{q}}^{\mathrm{T}}\boldsymbol{\lambda} - \mathbf{Q})_n = \mathbf{0} \\ \mathbf{F}^{(2)} = \dfrac{1}{\beta h^2}\mathbf{C}(\mathbf{q}_{n+1}, t_{n+1}) = \mathbf{0} \end{cases} \tag{4}$$

where $h = t_{n+1} - t_n$ is the step-size, n and $n+1$ refer to two consecutive time instants, and α and β are two parameters. The parameter α controls the amount of numerical damping that is added to the system. The smaller its value, the more numerical damping is added. In order to obtain a stable solution using the implicit HHT method, α must satisfy $-0.3 \leq \alpha \leq 0$. The parameter β is given by $(1-\alpha)^2/4$. Note that the constraint equation is scaled by $1/(\beta h^2)$ to get equation $\mathbf{F}^{(2)}$ in order to avoid a bad condition number of the Jacobian matrix in Eq. (5) when $h \to 0$.

Within the framework of the Newton-Raphson method, which can be adopted for solution of Eq. (4), at iteration k, the

following system of linear equations needs to be solved:

$$\begin{bmatrix} \dfrac{\partial \mathbf{F}^{(1)}}{\partial \ddot{\mathbf{q}}_{n+1}} & \dfrac{\partial \mathbf{F}^{(1)}}{\partial \boldsymbol{\lambda}_{n+1}} \\ \dfrac{\partial \mathbf{F}^{(2)}}{\partial \ddot{\mathbf{q}}_{n+1}} & \dfrac{\partial \mathbf{F}^{(2)}}{\partial \boldsymbol{\lambda}_{n+1}} \end{bmatrix}^{(k)} \begin{bmatrix} \boldsymbol{\Delta}\ddot{\mathbf{q}}_{n+1} \\ \boldsymbol{\Delta}\boldsymbol{\lambda}_{n+1} \end{bmatrix}^{(k)} = \begin{bmatrix} \dfrac{\partial \mathbf{F}^{(1)}}{\partial \ddot{\mathbf{q}}_{n+1}} & (\mathbf{C}_{\mathbf{q}}^{\mathrm{T}})_{n+1} \\ (\mathbf{C}_{\mathbf{q}})_{n+1} & \mathbf{0} \end{bmatrix}^{(k)} \begin{bmatrix} \boldsymbol{\Delta}\ddot{\mathbf{q}}_{n+1} \\ \boldsymbol{\Delta}\boldsymbol{\lambda}_{n+1} \end{bmatrix}^{(k)} = - \begin{bmatrix} \mathbf{F}^{(1)} \\ \mathbf{F}^{(2)} \end{bmatrix}^{(k)}. \tag{5}$$

The Jacobian $\partial \mathbf{F}^{(1)} / \partial \ddot{\mathbf{q}}_{n+1}$ is calculated by numerical differentiation. Whenever necessary, the numerical differentiation is performed through a complex-step derivative approximation (Martins *et al.*, 2003).

The algorithm is implemented with a variable time step size. The reader is referred to Hussein *et al.* (2008) for details.

2.1. Beam element

In this section, the finite element formulation is developed for the particular case of two-dimensional beam elements modeled according to the Euler-Bernoulli theory.

Figure 1 shows the beam element considered here. The nodal coordinates of the element are defined with respect to the inertial frame X_1X_2. The global position vector of a point on the elastic line of the beam is defined in terms of the element's nodal coordinates as:

$$\mathbf{r}(t,x) = \begin{Bmatrix} r_1 & r_2 \end{Bmatrix}^{\mathrm{T}} = \mathbf{S}(x)\mathbf{e}(t). \tag{6}$$

The shape function matrix and the vector of nodal coordinates of the element can be written as (Shabana, 2013):

$$\mathbf{S} = \begin{bmatrix} \left(1 - 3\xi^2 + 2\xi^3\right)\mathbf{I}_2 & l(\xi - 2\xi^2 + \xi^3)\mathbf{I}_2 & \left(3\xi^2 - 2\xi^3\right)\mathbf{I}_2 & l(\xi^3 - \xi^2)\mathbf{I}_2 \end{bmatrix}, \quad \mathbf{I}_2 = \begin{bmatrix} 1 & 0 \\ 0 & 1 \end{bmatrix}, \quad \xi = \frac{x}{l}, \tag{7}$$

and $\mathbf{e} = \begin{bmatrix} e_1 & e_2 & e_3 & e_4 & e_5 & e_6 & e_7 & e_8 \end{bmatrix}^{\mathrm{T}}$, with:

$$\begin{aligned} e_1 &= r_1|_{x=0}, \qquad e_2 = r_2|_{x=0}, \qquad e_3 = \left.\frac{\partial r_1}{\partial x}\right|_{x=0}, \qquad e_4 = \left.\frac{\partial r_2}{\partial x}\right|_{x=0}, \\ e_5 &= r_1|_{x=l}, \qquad e_6 = r_2|_{x=l}, \qquad e_7 = \left.\frac{\partial r_1}{\partial x}\right|_{x=l}, \qquad e_8 = \left.\frac{\partial r_2}{\partial x}\right|_{x=l}, \end{aligned} \tag{8}$$

with l being the underformed length of the beam.

Using Eqs. (2) and (7), the mass matrix of the beam element with mass m can be analytically evaluated as:

$$\mathbf{M}^e = m \begin{bmatrix} \frac{13}{35} & 0 & \frac{11l}{210} & 0 & \frac{9}{70} & 0 & -\frac{13l}{420} & 0 \\ & \frac{13}{35} & 0 & \frac{11l}{210} & 0 & \frac{9}{70} & 0 & -\frac{13l}{420} \\ & & \frac{l^2}{105} & 0 & \frac{13l}{420} & 0 & -\frac{l^2}{140} & 0 \\ & & & \frac{l^2}{105} & 0 & \frac{13l}{420} & 0 & -\frac{l^2}{140} \\ & & & & \frac{13}{35} & 0 & -\frac{11l}{210} & 0 \\ & \text{sym} & & & & \frac{13}{35} & 0 & -\frac{11l}{210} \\ & & & & & & \frac{l^2}{105} & 0 \\ & & & & & & & \frac{l^2}{105} \end{bmatrix}. \tag{9}$$

Regarding the modeling of the internal forces, several formulations can be found in the literature (Nachbagauer, 2014). The main aspects of the approach adopted here are summarized below. The reader is referred to Berzeri and Shabana

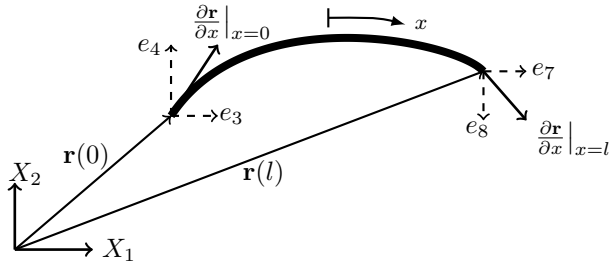

Figure 1: ANCF beam element under consideration.

(2000) and Berzeri *et al.* (2001) for additional details. The vector of internal forces related to the beam element can be expressed as:

$$\mathbf{F}^{\mathrm{int},e} = (\mathbf{K}_l^e + \mathbf{K}_t^e)\mathbf{e}, \tag{10}$$

where $\mathbf{K}_l^e$ and $\mathbf{K}_t^e$ are the longitudinal and transverse stiffness matrices, respectively. While the transverse stiffness matrix is linear, the longitudinal stiffness matrix is highly nonlinear on the nodal coordinates of the element. Their expressions are given below:

$$\mathbf{K}_t^e = \frac{EI}{l^3}\begin{bmatrix} 12 & 0 & 6l & 0 & -12 & 0 & 6l & 0 \\ & 12 & 0 & 6l & 0 & -12 & 0 & 6l \\ & & 4l^2 & 0 & -6l & 0 & 2l^2 & 0 \\ & & & 4l^2 & 0 & -6l & 0 & 2l^2 \\ & & & & 12 & 0 & -6l & 0 \\ & \text{sym} & & & & 12 & 0 & -6l \\ & & & & & & 4l^2 & 0 \\ & & & & & & & 4l^2 \end{bmatrix}, \quad \mathbf{K}_l^e = \frac{EA}{l}\begin{bmatrix} \mathscr{A} & 0 & \mathscr{B} & 0 & -\mathscr{A} & 0 & \mathscr{C} & 0 \\ & \mathscr{A} & 0 & \mathscr{B} & 0 & -\mathscr{A} & 0 & \mathscr{C} \\ & & \mathscr{D} & -\mathscr{B} & -\mathscr{A} & 0 & \mathscr{E} & 0 \\ & & & \mathscr{D} & 0 & -\mathscr{B} & 0 & \mathscr{E} \\ & & & & \mathscr{A} & 0 & -\mathscr{C} & 0 \\ & \text{sym} & & & & \mathscr{A} & 0 & -\mathscr{C} \\ & & & & & & \mathscr{F} & 0 \\ & & & & & & & \mathscr{F} \end{bmatrix}, \tag{11}$$

with:

$$\begin{aligned}
\mathscr{A} &= \frac{3}{70l^2}(a^2 + b^2 - 14l^2 - 6a_xd_x - 6b_xd_x - 6a_yd_y - 6b_yd_y + 24d^2) \\
\mathscr{B} &= \frac{1}{280l}(b^2 - a^2 + 2a_xb_x + 2a_yb_y - 14l^2 - 24a_xd_x - 24a_yd_y + 36d^2) \\
\mathscr{C} &= \frac{1}{280l}(a^2 - b^2 + 2a_xb_x + 2a_yb_y - 14l^2 - 24b_xd_x - 24b_yd_y + 36d^2) \\
\mathscr{D} &= \frac{1}{420}(12a^2 + b^2 - 3a_xb_x - 3a_yb_y - 28l^2 + 3a_xd_x - 3b_xd_x + 3a_yd_y - 3b_yd_y + 18d^2) \\
\mathscr{E} &= -\frac{1}{840}(3a^2 + 3b^2 - 4a_xb_x - 4a_yb_y - 14l^2 + 6a_xd_x + 6b_xd_x + 6a_yd_y + 6b_yd_y) \\
\mathscr{F} &= \frac{1}{420}(a^2 + 12b^2 - 3a_xb_x - 3a_yb_y - 28l^2 - 3a_xd_x + 3b_xd_x - 3a_yd_y + 3b_yd_y + 18d^2) \\
d_x &= e_5 - e_1, \quad d_y = e_6 - e_2, \quad a_x = le_3, \quad a_y = le_4, \quad b_x = le_7, \quad b_y = le_8, \\
d &= \sqrt{d_x^2 + d_y^2}, \quad a = \sqrt{a_x^2 + a_y^2}, \quad b = \sqrt{b_x^2 + b_y^2}
\end{aligned} \tag{12}$$

These expressions hold even for large deformations. In the previous equations, E is the Young's modulus of the material, I is the second moment of area and A is the cross-sectional area of the element, with all assumed to be constant.

3. POD-BASED MODEL ORDER REDUCTION

To promote a dimensionality reduction of the dynamic equations of motion, the proper orthogonal decomposition (POD) approach is used in this study. The POD is a data-driven strategy based on the singular value decomposition (SVD), which generates a set of orthogonal modes (the POD modes) that are optimal, in the sense of the Eckart-Young theorem (see Brunton and Kutz (2019)), for representing the simulation data, potentially allowing for a significant reduction of the number of modes needed to characterize the system dynamics, cf. Eq. (3).

To construct the POD modes, the set of equations given by Eq. (3) is numerically integrated over time. If $\mathbf{q}(t_k)$ is the vector of generalized coordinates at time t_k, the following snapshot matrix can be constructed from the simulation data:

$$\mathbf{X} = \left[\mathbf{q}(t_1) - \bar{\mathbf{q}} \quad \mathbf{q}(t_2) - \bar{\mathbf{q}} \quad \cdots \quad \mathbf{q}(t_m) - \bar{\mathbf{q}}\right], \tag{13}$$

where $\bar{\mathbf{q}}$ is the vector of time-averaged generalized coordinates. It is assumed that the m time instants are evenly spaced throughout the total simulation time. The system is assumed to be n-dimensional, so that $\mathbf{q} \in \mathbb{R}^n$ and $\mathbf{X} \in \mathbb{R}^{n\times m}$. Since the snapshot matrices considered throughout this paper are built from system responses (global position vectors and their gradients with respect to x), the discussion is limited to real matrices.

The SVD provides a unique matrix decomposition of the snapshot matrix in terms of the orthogonal matrices $\mathbf{U}$ and $\mathbf{V}$ and the matrix $\mathbf{\Sigma}$ with nonnegative entries on the diagonal, as follows:

$$\mathbf{X} = \mathbf{U}\mathbf{\Sigma}\mathbf{V}^{\mathrm{T}} = \begin{bmatrix}\boldsymbol{\psi}_1 & \boldsymbol{\psi}_2 & \cdots & \boldsymbol{\psi}_m\end{bmatrix}\begin{bmatrix}\sigma_1 & 0 & \cdots & 0 \\ 0 & \sigma_2 & & \vdots \\ \vdots & & \ddots & 0 \\ 0 & \cdots & 0 & \sigma_m\end{bmatrix}\begin{bmatrix}\mathbf{v}_1^{\mathrm{T}} \\ \vdots \\ \mathbf{v}_m^{\mathrm{T}}\end{bmatrix}, \tag{14}$$

where $\mathbf{U} \in \mathbb{R}^{n\times m}$, $\mathbf{\Sigma} \in \mathbb{R}^{m\times m}$ and $\mathbf{V} \in \mathbb{R}^{m\times m}$.

The matrix $\mathbf{\Sigma}$ is composed by the singular values of $\mathbf{X}$, σ_i, which are arranged in descending order. The energy content of $\mathbf{X}$ (defined according to the Frobenius norm) can be shown to be equal to the energy of its singular spectrum, $\Sigma_{i=1}^{m}\sigma_i^2$ (Kerschen and Golinval, 2002). Because of this, it follows that the matrix $\mathbf{U}$ provides the optimal set of modes to approximate $\mathbf{X}$ in a L_2-norm sense. The columns of this matrix contain the orthogonal POD modes necessary to form a basis to approximate the dynamics of interest. These modes are arranged from the most dominant to the least dominant, from left to right, in accordance with the organization of the singular values (descending order).

Thus, a low r-rank truncation can be obtained by selecting the first r-columns of $\mathbf{U}$ to construct the optimal basis modes, as follows (Brunton and Kutz, 2019):

$$\mathbf{\Psi} = \begin{bmatrix} \boldsymbol{\psi}_1 & \boldsymbol{\psi}_2 & \cdots & \boldsymbol{\psi}_r \end{bmatrix}, \tag{15}$$

where $\{\boldsymbol{\psi}_1, \ldots, \boldsymbol{\psi}_r\}$ are used to construct the orthogonal basis which is able to approximately capture the dynamic behavior which is described by Eq. (3).

Using these modes, it is possible to approximate the generalized coordinates $\mathbf{q}(t)$ of the system by means of:

$$\mathbf{q}(t) \approx \mathbf{\Psi}\boldsymbol{\xi}(t), \tag{16}$$

where $\boldsymbol{\xi} \in \mathbb{R}^r$ is the time-dependent vector of reduced generalized coordinates of the ROM. Thereafter, by using the Galerkin projection, Eq. (3) can be recast as the following set of equations with reduced order $r \ll n$:

$$\begin{cases} \mathbf{\Psi}^{\mathrm{T}}\mathbf{M}\mathbf{\Psi}\ddot{\boldsymbol{\xi}} + \mathbf{\Psi}^{\mathrm{T}}\mathbf{C}_{\mathbf{q}}^{\mathrm{T}}\boldsymbol{\lambda} = \mathbf{\Psi}^{\mathrm{T}}\mathbf{F}^{\mathrm{ext}}(t, \mathbf{\Psi}\boldsymbol{\xi}(t), \mathbf{\Psi}\dot{\boldsymbol{\xi}}(t)) - \mathbf{\Psi}^{\mathrm{T}}\mathbf{F}^{\mathrm{int}}(\mathbf{\Psi}\boldsymbol{\xi}(t)) = \mathbf{\Psi}^{\mathrm{T}}\mathbf{Q}(t, \mathbf{\Psi}\boldsymbol{\xi}(t), \mathbf{\Psi}\dot{\boldsymbol{\xi}}(t)) \\ \mathbf{C}(t, \mathbf{\Psi}\boldsymbol{\xi}(t)) = \mathbf{0} \end{cases} \tag{17}$$

Regarding the HHT-I3 numerical integration technique, Eq. (5) gets transformed to the following set of equations, with reduced order:

$$\begin{bmatrix} \mathbf{\Psi}^{\mathrm{T}}\dfrac{\partial \mathbf{F}^{(1)}}{\partial \ddot{\mathbf{q}}_{n+1}}\mathbf{\Psi} & \mathbf{\Psi}^{\mathrm{T}}(\mathbf{C}_{\mathbf{q}}^{\mathrm{T}})_{n+1} \\ (\mathbf{C}_{\mathbf{q}})_{n+1}\mathbf{\Psi} & \mathbf{0} \end{bmatrix}^{(k)} \begin{bmatrix} \boldsymbol{\Delta}\ddot{\boldsymbol{\xi}}_{n+1} \\ \boldsymbol{\Delta}\boldsymbol{\lambda}_{n+1} \end{bmatrix}^{(k)} = -\begin{bmatrix} \mathbf{\Psi}^{\mathrm{T}}\mathbf{F}^{(1)} \\ \mathbf{F}^{(2)} \end{bmatrix}^{(k)}. \tag{18}$$

Care has to be exercised regarding the algebraic constraint equations. It is known that the POD modes inherit some attributes present in the data used to construct them. This can lead to redundant constraint equations, which need to be taken care of. Since the snapshot matrix $\mathbf{X}$ in Eq. (13) is constructed from data gathered from the full-order system, the data set contains generalized coordinates that fully satisfy the constraint equations. As a result, the obtained POD modes contain constraint information, so that at least some constraint equations may be automatically satisfied in the low-dimensional subspace. This leads to singularities in the Jacobian matrix of Eq. (18), since $(\mathbf{C}_{\mathbf{q}})_{n+1}\mathbf{\Psi}$ (and, equivalently, $\mathbf{\Psi}^{\mathrm{T}}(\mathbf{C}_{\mathbf{q}}^{\mathrm{T}})_{n+1}$) may contain all-zero rows (columns). In order to remedy these singularities, a simple approach based on the work of Luo *et al.* (2017) is adopted in this study. Before starting numerical integration, the matrix $\mathbf{C}_{\mathbf{q}}\mathbf{\Psi}$ is evaluated for the initial time instant t_1. If an all-zero row is identified, the corresponding constraint equation and the associated Lagrange multiplier are eliminated from the problem. These constraint equations, and the corresponding constraint forces are no longer computed at any time in the ROM.

4. ADAPTATION OF ROMs TO ACCOUNT FOR MODEL PARAMETER VARIATIONS

Problems such as design optimization, uncertainty analysis, control, and many other applications generally involve repeated analysis under parameter changes. However, the above-discussed POD-based ROM lack robustness in such cases, as discussed by Amsallem and Farhat (2008). Therefore, performing dynamic calculations using ROMs calls for the construction of a new ROM every time a system parameter is varied.

In this study, an interpolation method based on the Grassmann manifold is applied for adapting ROMs to new sets of parameters. This method has been proposed and successfully applied in the fields of aeroelasticity and structural dynamics. Roughly speaking, the data to be interpolated is mapped onto a tangent space to the Grassmann manifold, then the mapped data is interpolated in this space, and, finally, the interpolated result is appropriately transported back to the original space. For more details, the reader is referred to (Amsallem and Farhat, 2008) and (Amsallem *et al.*, 2009). The implementation aspects of the interpolation algorithm, are depicted in Fig. 2, and described below.

1. The sampling points S_0, S_1, ..., S_k of the manifold are specified with respect to the parameters $\lambda_0, \lambda_1, \ldots, \lambda_k$, such that each sampling point S_i $(i = 0, 1, \ldots, k)$ corresponds to a matrix $\mathbf{U}_i$ $(i = 0, 1, \ldots, k)$ of POD modes of the same dimension.

2. A point S_0 of the manifold is chosen as a reference for the interpolation. It is noticed that the method is not sensitive to the choice of the reference point.

3. Each sampling point S_i is mapped to a point χ_i in the tangent space by using a matrix $\mathbf{\Psi}_i$ through the following logarithm map:

$$\begin{cases} \mathbf{L}_i \mathbf{\Sigma}_i \mathbf{R}_i^{\mathrm{T}} = (\mathbf{I} - \mathbf{U}_0 \mathbf{U}_0^{\mathrm{T}}) \mathbf{U}_i (\mathbf{U}_0^{\mathrm{T}} \mathbf{U}_i)^{-1} & \text{(economy-size SVD)} \\ \mathbf{\Psi}_i = \mathbf{L}_i \tan^{-1}(\mathbf{\Sigma}_i) \mathbf{R}_i^{\mathrm{T}} \end{cases} \tag{19}$$

4. A new point $\tilde{\chi}$, related to the desired parameter $\tilde{\lambda}$, is obtained by interpolating the points $\chi_0, \chi_1, \ldots, \chi_k$. In this work, the Lagrange interpolation formula is used to compute the matrix $\tilde{\mathbf{\Psi}}$ representing $\tilde{\chi}$. The Lagrange interpolation formula is given by:

$$\tilde{\mathbf{\Psi}} = \sum_{i=0}^{k} \left(\mathbf{\Psi}_i \prod_{\substack{0 \leq j \leq k \\ j \neq i}} \frac{\tilde{\lambda} - \lambda_j}{\lambda_i - \lambda_j} \right). \tag{20}$$

5. Lastly, the matrix $\tilde{\mathbf{\Psi}}$ is mapped from the tangential space back to the Grassmann manifold, so that one is able to obtain $\mathbf{U}_{\mathrm{new}}$, the matrix of POD modes associated with the parameter $\tilde{\lambda}$. This is achieved through the exponential map:

$$\begin{cases} \tilde{\mathbf{L}} \tilde{\mathbf{\Sigma}} \tilde{\mathbf{R}}^{\mathrm{T}} = \tilde{\mathbf{\Psi}} & \text{(economy-size SVD)} \\ \mathbf{U}_{\mathrm{new}} = \mathbf{U}_0 \tilde{\mathbf{R}} \cos(\tilde{\mathbf{\Sigma}}) + \tilde{\mathbf{L}} \sin(\tilde{\mathbf{\Sigma}}) \end{cases} \tag{21}$$

It is noteworthy that the important orthogonality property of the modes is kept. Once the matrix $\mathbf{U}_{\mathrm{new}}$ is obtained, the POD-based ROM can be constructed as discussed earlier.

5. NUMERICAL EXAMPLES

In this section, the above-discussed methodology is applied to the simulation of two multibody dynamics problems: a four-bar mechanism and a free-falling double pendulum. These are benchmark problems extensively studied and validated with other conceptually different flexible multibody dynamics formulations.

In all simulations, the numerical damping parameter α is set as -0.1. Although the numerical integrator has a variable time step, the results are presented with a time step of 1×10^{-3} s.

5.1. Four-bar mechanism

First, the multibody dynamic analysis of the four-bar mechanism shown in Fig. 3 is performed. The geometric, elastic, and inertial properties of the four-bar links are listed in Tab. 1 and are the same as used by Berzeri and Shabana (2000)

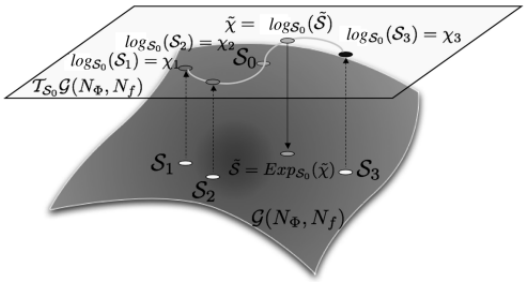

Figure 2: Graphical representation of the interpolation of four subspaces in a tangent space to a Grassmann manifold. Reprinted from Amsallem and Farhat (2008).

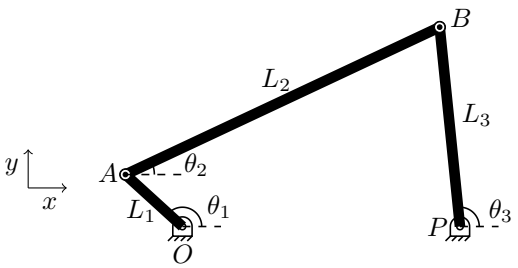

Figure 3: Four-bar mechanism under analysis.

and Kim *et al.* (2017). The crank, coupler and follower links are discretized using 20, 50 and 40 ANCF beam elements, respectively, resulting in a total of 452 degrees of freedom and 8 kinematic constraints. The system starts from rest with the orientation angles initially given by $\theta_1 = 0°$, $\theta_2 = 30°$ e $\theta_3 = 60°$, and is driven by a moment M_{applied} applied to the crank, expressed as (Yakoub and Shabana, 1999):

$$M_{\text{applied}} = \lambda \times \begin{cases} 10\sin(3\pi t)\ \text{Nm}, & t \leq 0.2728\ \text{s} \\ 465.8838298e^{-16.324194t}\ \text{Nm}, & t > 0.2728\ \text{s} \end{cases} \tag{22}$$

A parametric study is carried out by altering λ, which is varied by $0.25/0.5/0.75/1$ in the dynamic analyses which are conducted to construct the ROM of the system.

Figure 4 shows the y-position occupied by the revolute joint between the coupler and the follower (point B in Fig. 3). The plots presented in this figure illustrate some of the data which was used to obtain a ROM of the system.

Table 1: Geometric, elastic and inertial properties of the flexible four-bar links.

Property	**Link 1 (crank)**	**Link 2 (coupler)**	**Link 3 (follower)**
Number of elements	20	50	40
Length (m)	0.2	0.9	0.5196152
Mass (kg)	0.6811	2.4740	1.4700
Second moment of area (m^4)	1.257×10^{-7}	3.068×10^{-7}	3.976×10^{-8}
Cross-sectional area (m^2)	1.257×10^{-3}	1.960×10^{-3}	7.068×10^{-4}
Young's modulus (Pa)	1×10^{9}	5×10^{6}	5×10^{8}

After the construction of the ROM, a new dynamic analysis was performed with a randomly selected parameter $\lambda = 0.935$. The order of truncation of the POD modes matrices was chosen so that at least 99.9% of the variance of all simulations in the training set would be captured. In this way, the dynamic simulations were carried out via the ROM with 33 generalized coordinates, and none of the constraint equations. This represents a reduction of the order of the system of equations given in Eq. (5) by 92.8%.

The dynamic response of the four-bar mechanism considering the updated value for λ is shown in Fig. 6 for four equally spaced time instants. Figure 5 shows the y-position of the revolute joint between the coupler and the follower links for the ROM and the full-order model (FOM). It indicates a high degree of accuracy of the ROM over the analysis time.

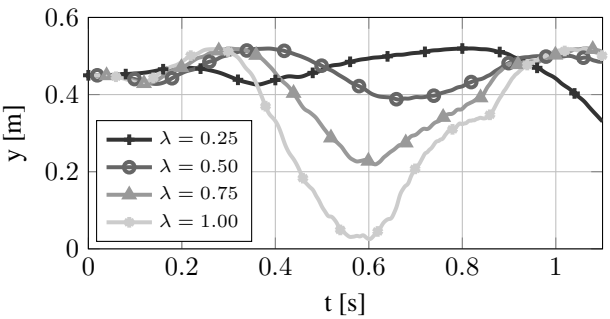

Figure 4: Y-position of the joint between the coupler and the follower for the training dynamic analyses.

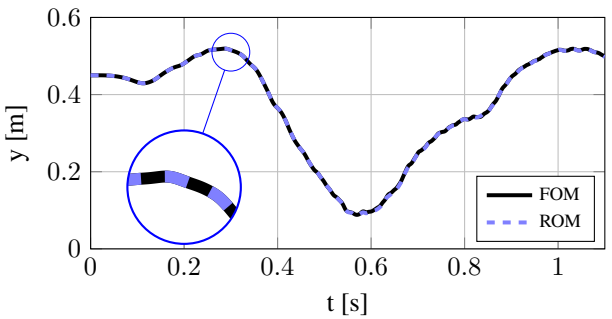

Figure 5: Y-position of the joint between the coupler and the follower links for the system under perturbation.

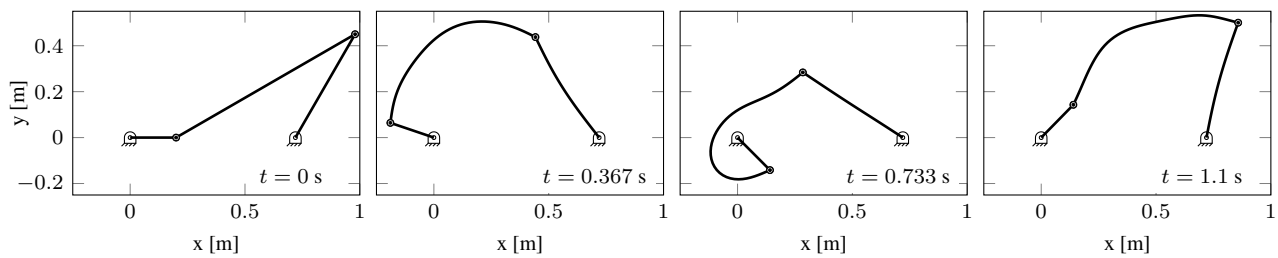

Figure 6: Evolution of the four-bar mechanism under analysis.

5.2. Free-falling double pendulum

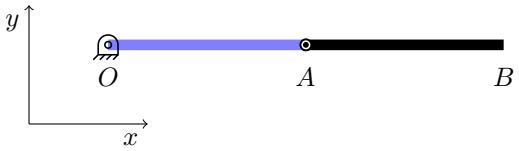

Figure 7: Double pendulum under analysis.

The second example considered here is related to a flexible double pendulum which experiments free fall under the action of its own weight (Fig. 7). The first pendulum is restrained to the ground through a pin joint at point O, and the two pendulums are connected by means of a pin joint at point A. The gray and red bodies have a Young's modulus of 80 MPa and 1 MPa, respectively. Both have a square cross-section with dimensions of 30 mm and a length of 0.5 m. The system begins to fall from an horizontal configuration, from rest, under gravity's influence ($g = 9.81$ m/s^2). Each pendulum is modeled using 80 ANCF beam elements, resulting in a total of 648 degrees of freedom and 4 kinematic constraints. Transient dynamic analyses are performed until the final time of 1.3 s.

The parametric study is carried out with respect to the mass of each body. The initial masses of the bodies are given by 0.304 kg and 0.2455 kg, respectively. For the construction of the parametric ROM, training dynamic analyses were performed by scaling the masses successively by the factors $0.5/1.0/1.5$, resulting in a total of 9 simulations (full-factorial experiment). Since there are two parameters to interpolate, the Lagrange interpolation formula given in Eq. (20) must be adapted to handle the two-dimensional case at hand. If two parameters $\lambda_i (i = 0, 1, \ldots, m)$ and $\eta_j (j = 0, 1, \ldots, n)$ are associated to the matrix $\tilde{\mathbf{\Psi}}_{ij}$, the matrix $\tilde{\mathbf{\Psi}}$ related to the desired parameters $\tilde{\lambda}$ and $\tilde{\eta}$ can be computed as:

$$\tilde{\mathbf{\Psi}} = \sum_{i=0}^{m} \sum_{j=0}^{n} \left(\mathbf{\Psi}_{ij} L_i(\tilde{\lambda}) L_j(\tilde{\eta}) \right), \qquad \text{where} \quad L_i(\tilde{\lambda}) = \prod_{\substack{s=0 \\ s \neq i}}^{m} \frac{\tilde{\lambda} - \lambda_s}{\lambda_i - \lambda_s}, \qquad L_j(\tilde{\eta}) = \prod_{\substack{s=0 \\ s \neq j}}^{n} \frac{\tilde{\eta} - \eta_s}{\eta_j - \eta_s}. \tag{23}$$

Figure 8 shows the time evolution of the y-position of the end point of the the double pendulum (point B in Fig. 7) for the dynamic analyses conducted to gather data for constructing the POD-based ROM.

After construction of the ROM, a new dynamic analysis was performed considering a randomly selected set of masses equal to 0.2642 kg and 0.1500 kg for bodies 1 and 2, respectively. The order of truncation of the POD modes matrices was chosen so that at least 99.9% of the variance of all simulations in the training set could be captured. In this way, the dynamic simulations were carried out using the ROM with 11 generalized coordinates, and none of the constraint equations. This represents a 98.3% reduction in the order of the system of equations given in Eq. (5).

Various postures assumed by the flexible double pendulum, whose links have the randomly selected masses, can be seen in Fig. 9. Figure 10 shows the time history of the y-position of the end point of the double pendulum, computed using the ROM and the FOM. The results of the two approaches match almost perfectly over the time period which has been considered.

It is interesting to investigate the behavior of the ROM over a longer time window than the one used to construct the snapshot matrix seen in Eq. (13). For such, additional simulations, with the same randomly selected set of masses, were performed considering the final time instant equal to 3.0 s. Figure 11 shows another comparison for the y-position of the tip of the flexible double pendulum, calculated using the ROM and the FOM. These simulation results are quite close to each other over the longer time window considered now.

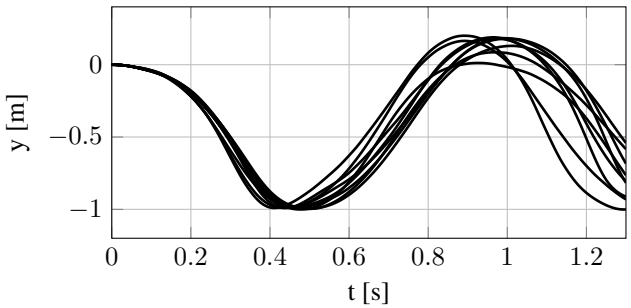

Figure 8: Y-position of the end point of the the double pendulum for the training dynamic analyses.

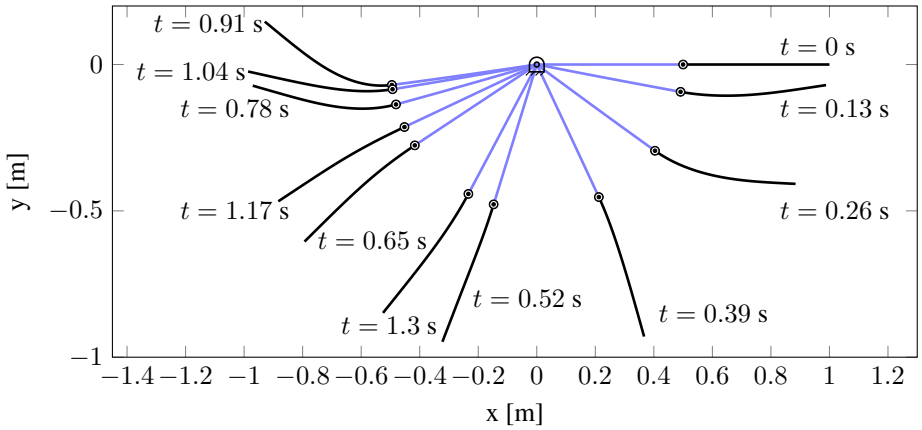

Figure 9: Evolution of the flexible double pendulum under analysis.

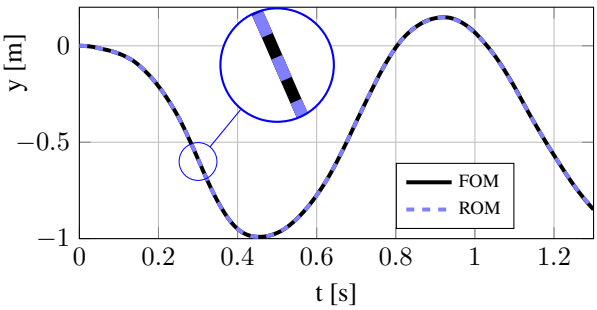

Figure 10: Y-position of the end point of the the double pendulum for the system with randomly selected masses.

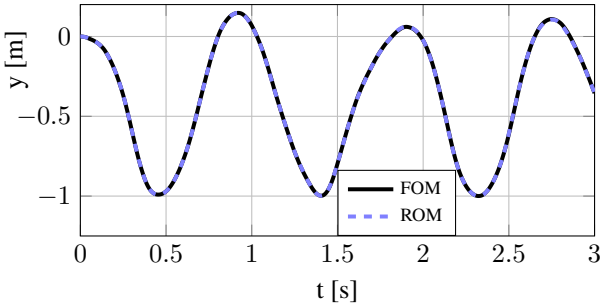

Figure 11: Y-position of the end point of the the double pendulum for the system with randomly selected masses. Simulation over a longer time window.

6. FINAL REMARKS

In this work, a method of parametric model order reduction is presented for the dynamic simulation of flexible multi-body systems based on the absolute nodal coordinate formulation. The reduced-order modeling is achieved using the proper orthogonal decomposition and Galerkin projection. The parametric ROM is obtained based on an interpolation procedure performed on a Grassmann manifold. The methodology is validated through the analysis of two flexible systems undergoing large reference motion and deformation, namely a four-bar mechanism, and a free-falling double pendulum. In order to avoid singularity problems, the redundant constraint equations resulting from the reduction of the model can be systematically detected and eliminated. The parametric ROMs proved to be able to reduce up to about 98% of the model order while maintaining great accuracy.

In future considerations, it is pertinent to investigate some method for sampling and interpolating the nonlinear terms present in the model, so that the computational cost of the ROM scale favorably with the order of the approximation, even with complex nonlinearities. Some possible candidates are the gappy POD, the discrete empirical interpolation method (DEIM), and the missing point estimation (MPE).

7. ACKNOWLEDGEMENTS

M.B.R.Fernandes is grateful to the São Paulo State Research Foundation (FAPESP) for his doctorate scholarship (grant #19/19921-5). M.B.R.Fernandes, T.P.Sales and D.A.Rade also acknowledge FAPESP for supporting their work through grant #18/15894-0 (Periodic structure design and optimization for enhanced vibroacoustic performance: ENVIBRO). D.A. Rade acknowledges the Brazilian Research Council (CNPq) for grants #310633/2013-3 and #312068/2020-4.

8. REFERENCES

Amsallem, D., Cortial, J., Carlberg, K. and Farhat, C., 2009. “A method for interpolating on manifolds structural dynamics reduced-order models”. *International Journal for Numerical Methods in Engineering*, Vol. 80, No. 9, pp. 1241–1258.

Amsallem, D. and Farhat, C., 2008. “Interpolation method for adapting reduced-order models and application to aeroelasticity”. *AIAA Journal*, Vol. 46, No. 7, pp. 1803–1813.

Arnold, M. and Brüls, O., 2007. “Convergence of the generalized-α scheme for constrained mechanical systems”. *Multi-*

body System Dynamics, Vol. 18, No. 2, pp. 185–202. ISSN 1573-272X.

Berzeri, M., Campanelli, M. and Shabana, A.A., 2001. "Definition of the elastic forces in the finite-element absolute nodal coordinate formulation and the floating frame of reference formulation". *Multibody System Dynamics*, Vol. 5, No. 1, pp. 21–54. ISSN 1573-272X.

Berzeri, M. and Shabana, A.A., 2000. "Development of simple models for the elastic forces in the absolute nodal co-ordinate formulation". *Journal of Sound and Vibration*, Vol. 235, No. 4, pp. 539 – 565. ISSN 0022-460X.

Brunton, S.L. and Kutz, J.N., 2019. *Data-Driven Science and Engineering: Machine Learning, Dynamical Systems, and Control*. Cambridge University Press.

Escalona, J., Hussien, H. and Shabana, A., 1998. "Application of the absolute nodal co-ordinate formulation to multibody system dynamics". *Journal of Sound and Vibration*, Vol. 214, No. 5, pp. 833 – 851. ISSN 0022-460X.

Gerstmayr, J., Sugiyama, H. and Mikkola, A., 2013. "Review on the absolute nodal coordinate formulation for large deformation analysis of multibody systems". *Journal of Computational and Nonlinear Dynamics*, Vol. 8, No. 3.

Hussein, B., Negrut, D. and Shabana, A.A., 2008. "Implicit and explicit integration in the solution of the absolute nodal coordinate differential/algebraic equations". *Nonlinear Dynamics*, Vol. 54, No. 4, pp. 283–296. ISSN 1573-269X.

Kerschen, G. and Golinval, J., 2002. "physical interpretation of the proper orthogonal modes using the singular value decomposition". *Journal of Sound and Vibration*, Vol. 249, No. 5, pp. 849–865.

Kerschen, G., Golinval, J.C., Vakakis, A.F. and Bergman, L.A., 2005. "The method of proper orthogonal decomposition for dynamical characterization and order reduction of mechanical systems: An overview". *Nonlinear Dynamics*, Vol. 41, No. 1-3, pp. 147–169.

Kim, E. and Cho, M., 2018. "Design of a planar multibody dynamic system with ANCF beam elements based on an element-wise stiffness evaluation procedure". *Structural and Multidisciplinary Optimization*, Vol. 58, No. 3, pp. 1095–1107.

Kim, E., Kim, H. and Cho, M., 2017. "Model order reduction of multibody system dynamics based on stiffness evaluation in the absolute nodal coordinate formulation". *Nonlinear Dynamics*, Vol. 87, No. 3, pp. 1901–1915.

Luo, K., Hu, H., Liu, C. and Tian, Q., 2017. "Model order reduction for dynamic simulation of a flexible multibody system via absolute nodal coordinate formulation". *Computer Methods in Applied Mechanics and Engineering*, Vol. 324, pp. 573 – 594. ISSN 0045-7825.

Martins, J.R.R.A., Sturdza, P. and Alonso, J.J., 2003. "The complex-step derivative approximation". *ACM Transactions on Mathematical Software*, Vol. 29, No. 3, pp. 245–262.

Nachbagauer, K., 2014. "State of the art of ancf elements regarding geometric description, interpolation strategies, definition of elastic forces, validation and the locking phenomenon in comparison with proposed beam finite elements". *Archives of Computational Methods in Engineering*, Vol. 21, No. 3, pp. 293 – 319.

Negrut, D., Jay, L.O. and Khude, N., 2009. "A discussion of low-order numerical integration formulas for rigid and flexible multibody dynamics". *Journal of Computational and Nonlinear Dynamics*, Vol. 4, No. 2, p. 021008.

Negrut, D., Rampalli, R., Ottarsson, G. and Sajdak, A., 2007. "On an implementation of the Hilber-Hughes-Taylor method in the context of index 3 differential-algebraic equations of multibody dynamics (DETC2005-85096)". *Journal of Computational and Nonlinear Dynamics*, Vol. 2, No. 1, p. 73.

Shabana, A.A., Hussien, H.A. and Escalona, J.L., 1998. "Application of the absolute nodal coordinate formulation to large rotation and large deformation problems". *Journal of Mechanical Design*, Vol. 120, No. 2, pp. 188–195. ISSN 1050-0472.

Shabana, A., 1997a. "Definition of the slopes and the finite element absolute nodal coordinate formulation". *Multibody System Dynamics*, Vol. 1, No. 3, pp. 339–348. ISSN 1573-272X.

Shabana, A., 2013. *Dynamics of Multibody Systems*. Cambridge University Press, 4th edition. ISBN 9781107435889.

Shabana, A.A., 1997b. "Flexible multibody dynamics: Review of past and recent developments". *Multibody System Dynamics*, Vol. 1, No. 2, pp. 189–222. ISSN 1573-272X.

Yakoub, R.Y. and Shabana, A.A., 1999. "Use of cholesky coordinates and the absolute nodal coordinate formulation in the computer simulation of flexible multibody systems". *Nonlinear Dynamics*, Vol. 20, No. 3, pp. 267–282.

9. RESPONSIBILITY NOTICE

The authors are solely responsible for the printed material included in this paper.